Published in final edited form as:
Neurobiol Dis. 2007 October ; 28(1): 39–51.

Axonal and Periaxonal Swelling Precede Peripheral Neurodegeneration in KCC3 Knockout Mice

Nellie Byun and **Eric Delpire**
Neuroscience Graduate Program, Department of Anesthesiology, Vanderbilt University Medical Center, Nashville, TN 37232

Abstract

We have previously reported CNS and locomotor deficits in KCC3 knockout mice, an animal model of agenesis of the corpus callosum associated with peripheral neuropathy (ACCPN) (Howard, et al., 2002)). To assess the role of KCC3 in peripheral axon and/or myelin development and maintenance, we determined its expression and performed a detailed morphometric analysis of sciatic nerves. Sciatic nerves of juvenile wild-type mice, but not in adult, express KCC3. In the knockout, Schwann cell/myelin development appears normal at P3, but axons are swollen. At P8 and into P30, some fibers accumulate fluid periaxonally. These initial swelling pathologies are followed by myelin degeneration in adult nerves, leading to reduction in nerve conduction velocity. Mutant mice also exhibit decreased sensitivity to noxious pain. This evidence for swollen axons and fluid-related axonopathy, which ultimately result in neurodegeneration, implicates cell volume regulation as a critical component of peripheral nerve maintenance.

Keywords

KCC3; Andermann syndrome; ACCPN; peripheral neuropathy; sciatic nerve; cell volume regulation; RVD; Schwann cell; axon; myelin

INTRODUCTION

Peripheral neuropathy and mental retardation are the pathological hallmarks of the neurological disorder ACCPN (OMIM 218000), and are often associated with variable agenesis of the corpus callosum (ACC), areflexia, and psychosis. The course of peripheral neuropathy, regardless of ACC, begins with hypotonia during infancy, delayed motor milestones, then wheelchair confinement in early adolescence (Dupre, et al., 2003; Howard, et al., 2002). Mutations in *SLC12A6* (solute carrier 12A6; human KCC3 gene) resulting in truncated nonfunctional protein were identified in ACCPN patients by single-strand conformation polymorphism analysis (Howard, et al., 2002).

In parallel to the genetic study, we produced KCC3 knockout mice that exhibited locomotor deficits by ~2 weeks, first low posture indicating limb weakness, then hindleg dragging. Poor performance on rotorod, wire-hang, and beam tasks and CNS deficits of significantly low

Address correspondence to: Eric Delpire, Department of Anesthesiology, T-4202 MCN 1161 21st Avenue South, Nasvhille, TN 37232-2520, Tel: 615 343-7409, Fax: 615 343-3916, E-mail: eric.delpire@vanderbilt.edu.

exploratory behavior and abnormal prepulse inhibition confirmed the mouse as a good model of ACCPN (Howard, et al., 2002). Boettger et al. found in their independent KCC3$^{-/-}$ line: hypertension, age-related deafness, increased seizure susceptibility, and a similar peripheral neuropathy phenotype (Boettger, et al., 2003).

KCC3 is one of four potassium-chloride cotransporters that mediate the coupled electroneutral movement of K^+ and Cl^- ions across plasma membranes (Jennings and Adame, 2001). Their classical roles include intracellular chloride concentration maintenance, epithelial transport, and cell volume regulation (Adragna, et al., 2004; Delpire and Mount, 2002). First reported by Hiki and coworkers (Hiki, et al., 1999; Mount, et al., 1999; Race, et al., 1999), KCC3 regulates renal tubule and hippocampal cell volume (Boettger, et al., 2003), and has been implicated in ion homeostasis (Boettger, et al., 2003) and cell proliferation (Hsu, et al., 2007; Shen, et al., 2000; Shen, et al., 2001). KCC3 is expressed in brain, spinal cord, and dorsal root ganglia (DRG) neurons (Boettger, et al., 2003; Pearson, et al., 2001), but despite its broad expression (kidney, heart, pancreas, muscle, lung) (Hiki, et al., 1999; Mount, et al., 1999; Pearson, et al., 2001), its loss of function predominantly involves the central and peripheral nervous systems (Dupre, et al., 2003; Howard, et al., 2002). The peripheral nerve pathology, however, remained puzzling since KCC3 expression had not yet been demonstrated in sciatic nerves (Boettger, et al., 2003; Pearson, et al., 2001).

To understand how disruption of KCC3 function leads to neurodegeneration in peripheral nerves, we determined its expression pattern and conducted a detailed morphometric analysis of KCC3$^{-/-}$ and KCC3$^{+/+}$ sciatic nerves for quantitative and ultrastructural comparisons. We hypothesized that KCC3 is expressed before adulthood, and show that sciatic nerves of juvenile mice, but not adult, express the cotransporter. Schwann cell/myelin appears normal in KCC3$^{-/-}$ nerves at P3, but axons are enlarged. Swollen axons and periaxonal fluid accumulation at P8 and P30 precede adult neurodegeneration and is compatible with the role of K-Cl cotransport in cell volume regulation. Axon loss and myelin degeneration ultimately results in decreased nerve conduction that likely underlies the neuropathy. We propose that impairment of the cell's volume regulatory mechanism contributes to the peripheral nerve pathology and neurophysiological deficits.

MATERIAL AND METHODS

Animals

KCC3$^{-/-}$ mice were generated through homologous recombination as described previously (Howard, et al., 2002). Mice were mated for more than 10 generations in the C57BL6 background. Mice were housed in a Vanderbilt University Medical Center animal facility, with a 12 hour light-dark cycle and *ad libitum* food and water access. All animal procedures followed the National Institutes of Health guidelines on the use of animals and were approved by the Vanderbilt University Institutional Animal Care and Use Committee.

Genotyping

Wild-type, heterozygote, and homozygote mice were generated from heterozygote KCC3$^{+/-}$ matings. DNA was isolated by clipping 1 mm of the tail from anesthetized mice, treating the tail clip with 200 μl of digestion solution (25 mM NaOH and 0.2 mM EDTA, pH ~12) for 20 min at 95°C, neutralizing the sample with 200 μl of a 40 mM Tris-HCl, pH ~5 solution, and after mixing, centrifuging the digested tail tissue for 6 min at 14,000 rpm. Genotyping was performed through separate PCRs with 1 μl of tail DNA to amplify fragments specific to KCC3 control and mutant genes using the following primers: control gene forward 5'-GAACTTTGTGTTGATTCCTTTGG-3' and reverse 5'-TCTCCTAACTCCATCTCCAGGG-3' primers; mutant gene forward 5'-

GAACTTTGTGTTGATTCCTTTGG-3' and reverse 5'-TACAACACACACTCCAACCTCCG-3' primers. The PCR reactions yield 371 bp and 290 bp fragments for control and mutant, respectively.

Semi-quantitative RT-PCR

Total RNA from freshly dissected sciatic nerves and brain (positive control) was extracted using an RNeasy Mini Kit (Qiagen, Valencia, CA) according to the manufacturer's instructions, and treated with RQ1 RNase-free DNase (Promega, Madison, WI) to prevent false positive results. Reverse transcription was performed using total RNA, random hexamers as primers, dNTPs, DTT, and Superscript II reverse transcriptase (Invitrogen, Carlsbad, CA). For PCR amplification oligonucleotide primer pairs specific to mouse KCC3 cDNA were synthesized (forward 5'-AGCTCAAGGCAGGAAAGGGA-3' and reverse 5'-TTGTGTTTCAT GCCTCCGAGG-3' to amplify a 765 bp fragment) and primers for mouse beta-actin cDNA (forward 5'-GTGGGCCGCCCTAGGCACCA 3' and reverse 5'-GATGTCAACGTCACACTTC ATGATG -3' to amplify a 560 bp fragment) as a positive control and internal standard.

Antibody generation

The first 132-amino acids of the C-terminal of mouse KCC3a were fused to GST using the vector pGEX-T (Pharmacia, Piscataway, NJ). The fusion protein was grown in *E. coli* and purified with glutathione-conjugated sepharose beads. Polyclonal antibodies were produced in two New Zealand white rabbits after subcutaneous injections of the GST-peptide (Covance, Denver, PA). The antiserum from the first production bleed was affinity-purified as described previously (Pearson, et al., 2001). The purified antibody was tested by immunoblot on mouse brain microsomes and lysates from wild-type and $KCC3^{-/-}$ mice. Because the antibody nonspecifically detected a large band (~300 kDa) in both wild-type and knockout, the antibody was further purified using a shorter fragment (amino acids 1-44) of the antigenic GST-peptide to remove nonspecific binding while still detecting the 155 kDa KCC3 protein band.

Microsomal Protein Isolation and Western Blot Analysis

Sciatic nerves and brains were dissected from euthanized mice and homogenized in a sucrose buffer (0.32 M sucrose, 5 mM Tris-HCl, pH 7.5, 2 mM EDTA) with a Teflon pestle. We obtained microsomal protein through successive centrifugations at 3000 *g*, 10,000 *g* and 100,000 *g*. Following resuspension of the high-speed pellet in a 5 mM Tris–HCl, pH 7.5/2 mM EDTA buffer, we determined protein concentrations using the Bradford assay (BioRad, Hercules, CA). Protein samples from microsomes were denatured in SDS-PAGE loading buffer at 75°C for 20 min and separated on a 9% polyacrylamide gel. After the proteins were electroblot-transferred from the gels onto polyvinylidine fluoride membranes (BioRad), the membranes were incubated for 2 h at room temperature (RT) in blocking solution made up of 5% non-fat dry milk in Tris-buffered saline with Tween 20 (TBST). Membranes were then incubated with primary antibody at 1:1000 dilution in blocking solution at 4°C overnight. Following TBST washes (3 h), membranes were incubated in horseradish peroxidase-conjugated anti-rabbit secondary antibody in blocking solution (1:4000; Jackson Immunoresearch, West Grove, PA) for 1 h at RT, and then rinsed for 2 h in TBST. Protein bands detected by antibody were visualized by chemiluminescence using ECL Plus (Amersham Biosciences, Arlington Heights, IL).

Schwann cell cultures

Primary rat Schwann cell cultures were prepared following the method of Yeiser et al. (Yeiser, et al., 2004). Sciatic nerves were dissected from P2-P3 rat pups, and following enzymatic digestion with 0.3% collagenase (37°C for 15 min) and 0.25% trypsin (37°C for 15 min). The

trypsin reaction was halted with DMEM with 10% FBS. After applying rat Schwann cell media (DMEM containing 10% FBS, 100 U/ml penicillin, and 100 μg/ml streptomycin), Schwann cells were dissociated by trituration, and pipetted into poly-L-lysine (Sigma, St. Louis, MO) coated 6-well plates. The following day, cultures were treated with Ara-C to remove fibroblasts.

Immunohistochemistry

Dissected spinal cord and dorsal root ganglia from P14 mice were fixed overnight at 4°C in fresh 4% paraformaldehyde, then cryoprotected in 30% sucrose in PBS. The following day, tissues were embedded in Tissue-Tek OCT compound (Sakura Finetek, Torrance, CA), frozen, sectioned into 12 μm thick slices on a Leica cryostat, and thaw mounted onto Superfrost Plus slides (Fisher Scientific, Pittsburg, PA). After drying, sections were washed in PBS, permeabilized with 1% SDS in PBS, blocked for 1 h in 1% BSA/5% goat serum in PBS, and then incubated overnight with purified polyclonal KCC3 antibodies (see above) in blocking solution (1:200) at 4°C. Antibody-treated sections were washed in PBS and incubated in Cy3-conjugated mouse anti-rabbit antibody (1:800) for one hour at RT. Following PBS washes, sections were mounted in VectaShield (Vector Laboratories, Burlingame, CA), coverslipped, and sealed. Teased sciatic nerves from P8 $KCC3^{+/+}$ and $KCC3^{-/-}$ pups were immunostained as described by Boyle et al (Boyle, et al., 2001), but with anti-KCC3 antibody (1:200) and Cy3-conjugated goat anti-rabbit secondary antibody (1:800). Fluorescence signal was visualized using a Carl Zeiss LMS 510 META confocal microscope.

Transmission Electron Microscopy (TEM)

Anesthetized adult mice were perfused intercardiacally with 0.1M sodium cacodylate buffer followed by 2.5% glutaraldehyde in sodium cacodylate. Sciatic nerves were dissected and post-fixed in fresh glutaraldehyde, then processed by the Vanderbilt EM Core. Nerves were washed in 0.1M sodium cacodylate buffer, post-fixed in 1% osmium tetroxide for 1 h, rinsed with sodium cacodylate buffer 3× 5 min, then dehydrated through an ethanol series (50% 5 min, 75% 15 min, 95% 2× 15 min, 100% 3× 20 min). Resin (1/2 propylene oxide-1/2 Spurr) was placed in a vacuum oven (18 psi) overnight, then changed into fresh Spurr and returned to the vacuum oven for 2 h. Samples were embedded in Spurr resin and incubated at 60°C for 24-48 h. Thick sections (500 nm) were examined after toluidine blue staining. For TEM, ultra-thin sections (80 nm) were placed on copper grids (Electron Microscopy Science, Hatfield, PA), and stained with uranyl acetate and lead citrate. Samples were viewed using a Philips CM-12 transmission electron microscope at 80kV. Photomicrographs for morphometric analysis were taken at 2650 magnification, by systematically covering adjacent but non-overlapping fields.

Morphometrical Analysis

Using TEM photomicrographs at 2650 magnification, we measured the diameters of sciatic nerve axons and fibers (axon and myelin sheath) using the free image analysis software ImageJ (NIH, http://rsb.info.nih.gov/ij/). Photomicrograph frames that were only partially filled with fascicle, wrinkled, or damaged were excluded from the analysis. Images were thresholded to allow the software to digitally trace inside the myelin sheath to measure axon area and outside the myelin sheath to measure the area of the entire fiber. Diameters were extrapolated from areas under the assumption that fibers were perfect circles, and G ratios (axon diameter/fiber diameter) were calculated. The numbers of myelinated, unmyelinated, and partially myelinated axons were also tallied. Periaxonal/intramyelinic fluid accumulation was also counted. At P8 and P30, proximal (location where the nerve exits the spinal cord) and distal (the bifurcation into separate tibial and peroneal components at the knee) sciatic nerve regions were morphometrically evaluated. For P3 and 7-8 month old mice, since no difference was observed between the two regions, data were combined to increase statistical power.

Nerve Conduction

Mice were anesthetized under constant oxygen and isoflurane flow using a vaporizer, and body temperature was maintained using a warming pad. Sciatic-tibial motor nerve conduction velocity (NCV) was determined by first stimulating distally at the knee using bipolar Nicolet 0.4 mm platinum subdermal needle electrodes (Viasys Healthcare, Yorba Linda, CA) at supramaximal stimulation, and then at the sciatic notch. Compound muscle action potentials were recorded at the foot muscles with bipolar needle electrodes and data acquired using a Nicolet VikingQuest Portable System (Viasys Healthcare) with stimulus duration at 0.02 ms, range 25mA. Electrodes were cleaned with 70% alcohol between animals. Latencies and traces were analyzed using the VikingQuest software. Latencies were measured from stimulus onset to maximum negative peak. Sciatic-tibial NCVs were calculated using the distances between the two points of stimulation along the nerve divided by the resultant latencies.

Hot plate

Mice were transferred to the testing room and allowed to acclimate for 1 h before testing. Nociception threshold was measured for each mouse using a hot plate (model 35D; IITC Corporation, Woodland Hills, CA) that was maintained at 52°C. The mouse was confined to the surface of the hot plate by a clear acrylic cylinder (15 cm in diameter and 12.5 cm high). To measure pain threshold, the latency to respond with either hind paw licking, shaking/fluttering, or jumping was measured with a stop watch. The mouse was then immediately removed from the hot plate and returned to its cage. Each animal was tested twice, with a one week interval between the two sessions.

Statistics

Comparisons between two genotypes in the evaluation of morphometric data (for axon diameter and G ratio means) from $KCC3^{+/+}$ and $KCC3^{-/-}$ mice at P3 and 7-8 months as well as the hot-plate assay were made using unpaired t-tests. Group statistical differences for morphometric data for proximal and distal $KCC3^{+/+}$ and $KCC3^{-/-}$ sciatic nerves at P8 and P30 as well as nerve conduction data were analyzed using one-way analysis of variance (ANOVA) followed by multiple comparison using the Tukey post test. We used GraphPad Prizm software (GraphPad Softward Inc., San Diego, CA) for all of our statistical analyses. $P < 0.05$ was considered significant.

RESULTS

KCC3 transcript is detected in DRG, Schwann cells, and early postnatal peripheral nerves

Previous reports indicating no KCC3 expression in sciatic nerves (Boettger, et al., 2003; Pearson, et al., 2001) appeared inconsistent with the peripheral nerve pathology of $KCC3^{-/-}$ mice and ACCPN patients. To explore this discrepancy, we investigated KCC3 expression in the sciatic nerve at different ages since only adult, E14, and P0 were previously assessed (Boettger, et al., 2003; Pearson, et al., 2001). Based on the early onset of locomotor symptoms in afflicted mice (~2 weeks) and patients (infancy), we hypothesized that KCC3 is expressed postnatally corresponding to rodent peripheral nerve development. We extracted RNA from sciatic nerves of P2, P5, P14, and adult mice for semi-quantitative RT-PCR. In agreement with other reports, KCC3 transcript is undetectable in adult sciatic nerve; however, KCC3 mRNA is present at ages P2-P14 (Figure 1A).

To investigate the Schwann cell component of the peripheral nerve, we established primary Schwann cell cultures from P3 rat pup sciatic nerves, and performed RT-PCR with RNA extracted from these cells. Cultured Schwann cells were positive for KCC3 transcript (Figure 1B). It has been previously shown that both PNS and CNS neurons express KCC3 (Boettger,

et al., 2003; Pearson, et al., 2001), so as expected, RT-PCR results confirmed that rat DRG were positive for KCC3 mRNA (Figure 1C).

KCC3 protein expression in sciatic nerves

After developing and purifying a new KCC3 antibody, we first tested its specificity by Western blot on microsomes isolated from wild-type and $KCC3^{-/-}$ mouse brains, and it detected the ~155kDa protein from control but not mutant samples. Since KCC3 is membrane-bound, we isolated microsome fractions for immunoblots to enrich for membrane proteins. Microsomes isolated from sciatic nerves were separated on SDS-polyacrylamide gels and immunoblotted using the polyclonal anti-KCC3 antibody. No band was apparent for adult sciatic nerves, but P4 sciatic nerve was positive for KCC3 protein, while the ~155 kDa band was barely detectable at P15 (Figure 1D). These results confirmed our RT-PCR data.

To determine whether the axon and/or Schwann cell component of the sciatic nerve expresses KCC3, we immunostained teased sciatic nerve fibers with the anti-KCC3 antibody. For immunostaining experiments, $KCC3^{-/-}$ tissues from littermates served as negative controls. Using confocal microscopy, we found that in teased fibers from P8 wild-type mice, KCC3 signal localized to Schwann cell bodies (Figures 2A-H), and at higher magnification found that it was predominantly perinuclear (Figures 2E-F). Optical sections through Schwann cells showed staining on cell body membranes and perinuclear regions, but not within axons or nuclei. Schwann cell bodies could be distinguished morphologically in DIC images as rounded protrusions along fibers (Figures 2B, D, F, H). Only Schwann cell bodies exhibited strong staining, and KCC3 was not localized to specific subcellular regions of myelin or axon such as Schmidt-Lanterman incisures, nodes, juxtaparanodes, or paranodes. There was no staining in teased sciatic nerves from $KCC3^{-/-}$ littermates (2G-H), which were processed at the same time, nor in wild-type teased fibers treated only with secondary antibody (Figure 2C-D). KCC3 staining of DRG neurons, which were identified morphologically, was both membrane and intracellular (Figure 2I-J). As expected, KCC3 is expressed by the cell bodies of peripheral axons.

Mutant mice initiate myelination correctly but axons are enlarged

Hypomyelination in adult vertebrate peripheral nerves suggests a developmental defect in the myelination process that has led to thin sheaths (Hu, et al., 2006; Michailov, et al., 2004; Runker, et al., 2004; Warner, et al., 1996). Also, thin myelin in adult nerves is characteristic of regenerating axons after damage (Smith, et al., 1982). Since we had observed thin myelin sheaths around large axons, which could possibly represent hypomyelination, and myelin debris in adult $KCC3^{-/-}$ sciatic nerves (Howard, et al., 2002), we asked if KCC3 is involved in the ensheathing process during development. To determine the role of KCC3 in axon and/or myelin growth and maintenance and follow the pathogenesis of $KCC3^{-/-}$ sciatic nerves, we quantitatively compared these processes in $KCC3^{-/-}$ and wild-type mice by utilizing electron microscopy to conduct morphometric and ultrastructural analyses. In cross-section, myelin appears as a multilamellar structure circling axons, and software, such as ImageJ, can measure the area of an axon (area within the myelin sheath) and fiber (area of axon plus the myelin sheath) from which diameters can be extrapolated. The high contrast of nerve sections from osmium tetroxide staining allows the software to distinguish myelin, stained black, from other regions of the nerve.

At P3, just after the onset of myelination, $KCC3^{-/-}$ Schwann cells had essentially correctly segregated all large-caliber axons in a 1:1 relationship, and myelination was proceeding as in $KCC3^{+/+}$ littermates (Figure 3A-B). Although $KCC3^{-/-}$ nerve cross-sections appeared normal and undistinguishable from those of wild-type in EM photomicrographs, the average axon diameter was larger for $KCC3^{-/-}$ mice (Table 1). The increased mean diameters of $KCC3^{-/-}$

axons were due to a shift in the entire population of axons, which is graphically indicated by the histogram shift to the right (Figure 3C). There was no significant difference between mean G ratios at this age (Table 1) and G ratio scatter plots did not indicate hypomyelination (Figure 3D). On G ratio-axon diameter scatterplots, general hypomyelination would be represented as an upward shift of the entire regression line (Hu, et al., 2006; Michailov, et al., 2004), which is an increase in the y-intercept value without intersection of regression lines being compared.

Possible explanations for increased axonal caliber between littermates include advanced development or swelling. To check whether sciatic nerve development proceeded faster in $KCC3^{-/-}$ mice, we tallied the numbers of completely myelinated, partially myelinated, and segregated but unmyelinated axons (axons in Remak bundles were not counted), since a more mature nerve should have a higher ratio of myelinated axons. We found no difference between the two genotypes (Figure 3E), thus conclude that nerve development is not expedited, but rather, $KCC3^{-/-}$ axons are larger due to swelling. Equivalent densities of myelinated and total axons between wild-type and $KCC3^{-/-}$ sciatic nerves (Figure 3F) indicated normal axon numbers and migration.

$KCC3^{-/-}$ fibers accumulate fluid

We analyzed P8 sciatic nerves at two regions: (1) the bifurcation into separate tibial and peroneal components at the knee, which we labeled as distal; and (2) location where the nerve emanates from the spinal cord, which we labeled as proximal. The most striking ultrastructural finding was the presence of significantly enlarged fibers in mutant nerves (Figure 4D, Supplementary Figure 1). Examination of electron micrographs revealed that these enlarged fibers were not due to enlarged axons, but rather, to the widening of the periaxonal space that is electron-transparent and presumably fluid-filled (Figures 4D-H). The denser neurofilament and microtubule packing in affected fibers may be due to degeneration or compression. Myelinated fibers of both distal and proximal sciatic nerve were affected ($2.55 \pm 0.67\%$ and 1.23 ± 0.48 %, respectively) (see Table 1). We observed different degrees of severity or stages of fluid filling in the periaxonal space (Figures 4E-H) while intramyelinic fluid (data not shown) was rare. Some affected fibers contained myelin debris (Figure 4E, G). Clearly the periaxonal space has expanded beyond its normal spacing of 12-14 nm (Trapp, et al., 1984). The fluid in the periaxonal space separated the axolemma from the Schwann cell, but surprisingly, the myelin remained intact and accommodated the fluid build-up. Although internal myelin figures and debris were found in both wild-type and mutant fibers (Figure 4E), control nerves never showed periaxonal or intramyelinic fluid accumulation (Table 1). Ultrastructurally, there were no visible defects in compact myelin in mutant mice, indicating normal compaction as in wild-type (Figure 4C-D, insets).

Although most $KCC3^{-/-}$ fibers surrounding those with periaxonal swelling appeared qualitatively normal, our morphometry results indicate a subtle but significant defect. Mean axon diameters were larger for $KCC3^{-/-}$ axons compared to wild-type in both regions (Table 1). The general enlargement of the entire population of $KCC3^{-/-}$ axons indicated by the histogram shift was more prominent in distal (Figure 5C) than proximal nerve (Figure 5B). The higher mean G ratio of distal $KCC3^{-/-}$ fibers than in wild-type (Table 1) is reflected by the steeper G ratio scatter plot regression slope (Figure 5D). Since $KCC3^{-/-}$ axons at this age are of larger calibers as a population, there is no hypomyelination *per se*, but the appearance of thin myelin since the axon enlargement skews G ratios to higher values. Mean G ratios, however, were similar between mutant and wild-type fibers in proximal sciatic nerve. Note that fluid-filled fibers were not included in any G ratio plots, histograms, or calculations for mean axon diameters and G ratios since we were investigating underlying pathologies in $KCC3^{-/-}$ fibers with normal appearances.

KCC3$^{-/-}$ young adult nerves

At P30, increased axon diameters and periaxonal fluid pathologies remained in sciatic nerves of mutant mice (Supplementary Figure 2D). The significantly greater mean axon diameter for KCC3$^{-/-}$ than wild-type proximally (Table 1) is represented by the shift to the right of the entire mutant axon size distribution (Figure 6A). Unexpectedly, for distal sciatic nerve the histograms for the two genotypes now overlapped (Figure 6C) and mean axon calibers were not significantly different (Table 1). KCC3$^{-/-}$ fibers still exhibited periaxonal fluid accumulation (5.53 ± 3.8 % distally; 4.57 ± 2.3 % of proximally) albeit with wide variability. We also observed evidence of myelin deterioration, such as myelin-laden macrophages (Supplementary Figure 2D).

Neurodegeneration in older murine adult sciatic nerves

Previously, we had described defects such as thin myelin sheaths and myelin debris in transverse toluidene blue stained sections of KCC3$^{-/-}$ adult sciatic nerve (Howard, et al., 2002). In this study, electron microscopy confirmed the degeneration (Figure 7B-E), but the most prominent abnormality in the knockout were the presence of bands of Büngner (Figure 7C), which were not observed in wild-type sciatic nerve sections (Figure 7A). Denervation leaves behind the Büngner bands, which are arrays of Schwann cell processes that provide substrate for regenerating axons. The dying-back of axons after injury, or Wallerian degeneration, is followed by sprouting of new axons through the neural tube in the PNS, which KCC3$^{-/-}$ sciatic nerves exhibit. Indeed, 11.24 ± 1.84% of total myelinated axons was in regenerating clusters. The thinly myelinated axons that lie in regenerating clusters are evidence of axon degeneration followed by regrowth (Figure 7B). We also observed myelin and lipid debris within scavenging macrophages (Figure 7D-E). Myelinating Schwann cells were differentiated from macrophages by the presence of basal lamina, which macrophages do not produce. Macrophages, however, can invade a Schwann cell or neural tube, but when this was suspected, we re-examined the region at even higher magnification with EM. We observed layers of basal lamina surrounding some myelinated axons, (Figure 7B, D-E), which are Schwann cell remnants that indicate continuous Schwann cell activity of cell death and remyelination; however, we did not observe onion bulbs in sciatic nerves of either genotype. Although there was no difference in G ratio scatter plots between the two genotypes (Figure 7F) and axon diameter histograms overlapped (data not shown), there was clear evidence of axon loss at 7-8 months old, which was not apparent at early postnatal ages or even at P30. In older knockout animals, the frequency of periaxonal/intramyelinic fluid accumulation was 1.14 ± 0.46% (Table 1).

Nerve conduction and pain perception measurements

To test whether the morphological abnormalities in the adult knockout mouse result in a change in nerve conduction velocity (NCV), we measured compound muscle action potentials (CMAPs) (Figures 8A-B) at the foot muscle after stimulation at the knee and sciatic notch to determine sciatic-tibial conduction velocities for all three genotypes. The sciatic nerve is a mixed motor-sensory nerve. Since the output of nerve stimulation was muscle response (CMAP), we were solely evaluating the motor component. As indicated in Figure 8C, motor NCVs were significantly reduced in KCC3$^{-/-}$ mice, compared to heterozygote and wild-type mice (Table 1).

We utilized the standard hot plate test to evaluate pain threshold in KCC3$^{-/-}$ mice. Since the knockout mice have weak hind limbs, they may not be able to lick their hind paws as easily as wild-type mice, so we included shaking, fluttering, lifting of hind paws, and jumping as nociceptive withdrawal reflexes for both genotypes. Although KCC3$^{-/-}$ mice rarely licked their hind paws on this test, they were able to display the other discomfort responses, including jumping. KCC3 knockout mice exhibited impaired pain perception in the 52°C plate assay as

demonstrated by longer response latencies (Figure 8D). Noxious temperatures are carried by unmyelinated fibers, so the sensory defect of KCC3$^{-/-}$ mice point to possible changes in unmyelinated fibers.

DISCUSSION

The knockout mouse phenotype and devastating clinical features of ACCPN indicate an essential role of KCC3 in the nervous system. Our study provides a first comprehensive examination of the peripheral neuropathy component of ACCPN by investigating KCC3 expression in the PNS and utilizing a KCC3$^{-/-}$ mouse model for morphometric analyses. Although previous studies reported lack of KCC3 expression in E14, P0, and adult sciatic nerve (Boettger, et al., 2003; Pearson, et al., 2001), we show that KCC3 is expressed in sciatic nerves of juvenile mice and by Schwann cells. We also confirm KCC3 expression in DRG neurons. Although sciatic nerve development appears normal at P3, with KCC3$^{-/-}$ axons and Schwann cells undistinguishable from that of KCC3$^{-/-}$, axons are enlarged. Axon swelling continued into P8 and P30; however, periaxonal fluid accumulation was the most striking defect. In adult KCC3$^{-/-}$ nerves, we confirmed the occurrence of neurodegeneration, and specifically show evidence of axonal loss. The results, which are compatible with the role of KCC3 in cell volume regulation, lead to our proposal that the volume regulatory mechanism of KCC3 is necessary for peripheral nerve maintenance and function.

The early expression of KCC3 led to the original hypothesis that the cotransporter is involved in peripheral nerve development. However, based on the normal Schwann cell:axon segregation and initiation, and equivalent axon densities between the two genotypes, KCC3 does not regulate axon migration or myelination. The ultrastructural evidence of normal myelin compaction at all ages (as in P8, Figure 4C-D, insets) confirms normal development and shows that KCC3 is not involved in the dehydration process during myelin compaction.

The most dramatic and characteristic feature of all KCC3$^{-/-}$ sciatic nerves, never observed in wild-type, is the periaxonal fluid accumulation. Only a minority of fibers (at most 5%) exhibited periaxonal swelling, suggesting that only a small subset is affected. However, the defect is undercounted since we analyzed cross-sections, and the swelling is focal and distributed along the length of the myelinated fiber (see supplemental Figure 1). The fact that periaxonal swelling is found both proximally and distally also supports that the defect is distributed along the nerve. Furthermore, the possibility that only a subset of myelinating Schwann cells express KCC3 is unlikely, based on our immunostaining results (Figures 2A-B). However, the fact that the periaxonal swelling does not occur at every single internode, suggests that not all Schwann cells face stress conditions leading to KCC3 activation.

Fluid trapped in the periaxonal space appears to be a defect involving the Schwann cell's inability to extrude ions/fluid, ultimately disrupting axon-glial contacts necessary for the maintenance and survival of both. Numerous studies of knockout mice with disruptions of PNS proteins show that the two types of defects leading to abnormal periaxonal enlargement are 1) loss of proteins mediating axon-glial contacts, such as myelin-associated glycoprotein (Trapp, et al., 1984), and 2) inactivation/mutations of proteins involved in ion movement, such as C×32 (Anzini, et al., 1997; Scherer, et al., 1998). The periaxonal defect of C×32$^{-/-}$ mice show that ion dysregulation, i.e., disruption uptake of ions and fluid from the periaxonal space, attributed to potassium buffering, demonstrate the importance of ion/fluid clearance of Schwann cells. Although the C×32 model supports a defect in the uptake and transport of ions/fluid from the periaxonal space, based on its localization, KCC3 localization supports a role in the extrusion of ions and fluid from the Schwann cell body. This phenomenon is also observed in CNS where periaxonal fluid accumulation is observed in the C×47 knockout mouse and worst in the C×32/C×47-null mice (Menichella, et al., 2003; Menichella, et al., 2006). Furthermore, the severity

of phenotype, indicated by the number of swollen fibers and extent of swelling, increased with repetitive nerve activity. This indicates that the ion buffering capacity by glial cells is critical in nerve ions/fluid homeostasis, relevant to KCC3$^{-/-}$ fibers which exhibit similar periaxonal swelling.

By following the course of the disorder morphometrically, we also showed evidence for axonal swelling preceding the neurodegeneration in adult KCC3$^{-/-}$ mice. Not only was axonal swelling demonstrated by the increased mean diameters of KCC3$^{-/-}$ axons, but histogram analysis of axon diameters at ages P3, P8, and P30 also showed that axons without periaxonal fluid accumulation are enlarged as a population. Even at P3 when periaxonal swelling is not observed, axons are swollen. Unlike other examples of axonal swelling, such as giant axonal neuropathy (GAN patients and gigaxonin-null mice) and Charcot Marie Tooth disease 2E, which involve excessive neurofilament accumulation (Ding, et al., 2006; Fabrizi, et al., 2004; Fabrizi, et al., 2007; Yang, et al., 2007), KCC3$^{-/-}$ fibers show decreased cytoskeletal density compared to wild-type, supporting fluid accumulation.

Axonal swelling in KCC3$^{-/-}$ nerves was unexpected since cotransporter expression was not detected on the axolemma. However, since the axonal space is contiguous to the cell body, neuronal volume regulation defects in the soma, as observed in hippocampal KCC3$^{-/-}$ neurons (Boettger, et al., 2003)], could impact the volume of axons. Indeed, KCC3 is expressed in both spinal motor and DRG neurons throughout development and into adulthood (Boettger, et al., 2003), Alternatively, although we did not detect KCC3 staining in axons, we cannot rule out axonal expression at levels below our immunostaining detection sensitivity. Only immuno-gold electron microscopy would provide enough resolution to detect low KCC3 expression levels. Also, since various immunostaining studies have demonstrated the intracellular localization KCC3 (Boettger, et al., 2003; Mercado, et al., 2005; Pearson, et al., 2001), whether the cotransporter is recruited to the plasma membrane during cellular stress needs to be addressed.

Intriguingly, in older mice, when cotransporter transcript and protein become undetectable in wild-type mice, the axon diameter histograms for KCC3$^{-/-}$ and wild-type nerves overlap, which seems to indicate recovery from axonal swelling. This recovery could originate from the expression of another volume-activated transport mechanism in neurons/axons, and compensate for the lack of KCC3. In fact, we have previously shown expression of KCC4 in adult sciatic nerve (Karadsheh, et al., 2004). Since older wild-type mice do not express KCC3, the neurodegeneration seen in KCC3$^{-/-}$ nerves suggest that the cotransporter might be re-expressed upon injury. This hypothesis could be tested using nerve transection or constriction injury models.

The loss of axons in adult KCC3-null sciatic nerves is compatible with decreased sciatic motor nerve conduction velocity. Regenerating clusters and bands of Büngner in KCC3$^{-/-}$ sciatic nerves are evidence of axon loss, albeit with attempts to re-grow, as in Wallerian degeneration. Adolescent mice (P30) which histologically do not show axonal degeneration, however, also perform poorly on standard motor and balance tests (Howard, et al., 2002). This indicates that the earlier sciatic nerve defects, which are axonal enlargement and periaxonal swelling, can already impair motor and balance functions. Furthermore, the significantly higher pain threshold measured in KCC3$^{-/-}$mice compared to wild-type on the hot-plate test matches the clinical findings of sensory neuropathy in ACCPN patients. Abnormalities in both ventral and dorsal roots of KCC3$^{-/-}$mice indicate the involvement of both motor and sensory fibers (Boettger et al., 2003). Since noxious pain is transduced via unmyelinated fibers, this supports the finding of sensory fiber involvement in the knockout. Although we did not observe any obvious abnormalities in the Remak bundles of the sciatic nerve, whether or not unmyelianted axons also undergo swelling is unknown and could be evaluated by morphometric analysis.

However, as the hot-plate-evoked-pain response occurs through a supraspinal pathway, conduction and/or processing of pain sensory information can occur at multiple levels, including the CNS. Therefore, the pain phenotype could also originate from outside the peripheral nervous system.

Myelin and axonal disorders make up a large group of human neurological diseases and to this day are incurable. Although peripheral neuropathies can have varying etiologies (hereditary, diabetes, autoimmune, infectious, toxin, malnutrition) defective mechanisms in either axon, Schwann cell, or both precipitate these disorders. Mouse models have been important for studying the pathogenesis, genetics, and cellular/molecular mechanisms of those disorders. Whether the phenotype of $KCC3^{-/-}$ mice is predominantly driven by neuronal or Schwann cell defects remain to be studied and can be achieved by creating tissue-specific knockout mice. Our data show the importance of KCC3 function in the maintenance of peripheral nerves, likely through cell volume and fluid regulation. Cell swelling typically points to the blockade of an efflux pathway, consistent with K-Cl cotransporter function. Indeed, cell swelling triggers K^+ and Cl^- efflux through KCCs as well as K^+ and Cl^- channels (Lang, et al., 1998), so a diminished RVD response from the loss or inactivation of resident volume regulating proteins, such as KCC3, results in sustained swelling (Boettger, et al., 2003; Lauf and Adragna, 2000). The two early defects, axon and periaxonal swelling, followed by neurodegeneration may explain the progressive nature of the peripheral neuropathy. We also show that the early onset peripheral neuropathy of ACCPN is a neurodegenerative primary axonal disorder with myelin involvement. Additional animal models should allow us to determine whether the restoration of KCC3 function in childhood or early adulthood could reverse or ameliorate some of the ACCPN symptoms.

Supplementary Material

Refer to Web version on PubMed Central for supplementary material.

Acknowledgements

This work was supported by a pre-doctoral Ruth Kirschstein National Research Service Award (NRSA) training grant NS048633 to N.B., and NIH grant NS36758 to E.D. Experiments were performed in part through the use of the VUMC Research EM Resource (sponsored by NIH grants DK20539, CA68485, and DK58404) and we thank the EM Core for their technical expertise, as well as the Vanderbilt Cell Imaging Resource (supported by NIH grants CA68485 and DK20593) for the use and support on the confocal microscope; Lisa Diehl and Nathan Polley for genotyping the mice. We also wish to thank Dr. Amanda Peltier for the training and use of portable EMG equipment and discussions related to nerve conduction; Dr. Bruce Carter for the training in his laboratory for primary Schwann cell cultures; and Dr. Kenneth Gagnon for his help in generating GST fusion peptides and for discussion and critical reading of this manuscript.

References

Adragna NC, Fulvio MD, Lauf PK. Regulation of K-Cl cotransport: from function to genes. J Membr Biol 2004;201:109–137. [PubMed: 15711773]

Anzini P, Neuberg DH, Schachner M, Nelles E, Willecke K, Zielasek J, Toyka KV, Suter U, Martini R. Structural abnormalities and deficient maintenance of peripheral nerve myelin in mice lacking the gap junction protein connexin 32. J Neurosci 1997;17:4545–4551. [PubMed: 9169515]

Boettger T, Rust MB, Maier H, Seidenbecher T, Schweizer M, Keating DJ, Faulhaber J, Ehmke H, Pfeffer C, Scheel O, Lemcke B, Horst J, Leuwer R, Pape HC, Volkl H, Hubner CA, Jentsch TJ. Loss of K-Cl co-transporter KCC3 causes deafness, neurodegeneration and reduced seizure threshold. Embo J 2003;22:5422–5434. [PubMed: 14532115]

Boyle ME, Berglund EO, Murai KK, Weber L, Peles E, Ranscht B. Contactin orchestrates assembly of the septate-like junctions at the paranode in myelinated peripheral nerve. Neuron 2001;30:385–397. [PubMed: 11395001]

Delpire E, Mount DB. Human and murine phenotypes associated with defects in cation-chloride cotransport. Annu Rev Physiol 2002;64:803–843. [PubMed: 11826289]

Ding J, Allen E, Wang W, Valle A, Wu C, Nardine T, Cui B, Yi J, Taylor A, Jeon NL, Chu S, So Y, Vogel H, Tolwani R, Mobley W, Yang Y. Gene targeting of GAN in mouse causes a toxic accumulation of microtubule-associated protein 8 and impaired retrograde axonal transport. Hum Mol Genet 2006;15:1451–1463. [PubMed: 16565160]

Dupre N, Howard HC, Mathieu J, Karpati G, Vanasse M, Bouchard JP, Carpenter S, Rouleau GA. Hereditary motor and sensory neuropathy with agenesis of the corpus callosum. Ann Neurol 2003;54:9–18. [PubMed: 12838516]

Fabrizi GM, Cavallaro T, Angiari C, Bertolasi L, Cabrini I, Ferrarini M, Rizzuto N. Giant axon and neurofilament accumulation in Charcot-Marie-Tooth disease type 2E. Neurology 2004;62:1429–1431. [PubMed: 15111691]

Fabrizi GM, Cavallaro T, Angiari C, Cabrini I, Taioli F, Malerba G, Bertolasi L, Rizzuto N. Charcot-Marie-Tooth disease type 2E, a disorder of the cytoskeleton. Brain 2007;130:394–403. [PubMed: 17052987]

Hiki K, D'Andrea RJ, Furze J, Crawford J, Woollatt E, Sutherland GR, Vadas MA, Gamble JR. Cloning, characterization, and chromosomal location of a novel human K+-Cl- cotransporter. J Biol Chem 1999;274:10661–10667. [PubMed: 10187864]

Howard HC, Mount DB, Rochefort D, Byun N, Dupre N, Lu J, Fan X, Song L, Riviere JB, Prevost C, Horst J, Simonati A, Lemcke B, Welch R, England R, Zhan FQ, Mercado A, Siesser WB, George AL Jr, McDonald MP, Bouchard JP, Mathieu J, Delpire E, Rouleau GA. The K-Cl cotransporter KCC3 is mutant in a severe peripheral neuropathy associated with agenesis of the corpus callosum. Nat Genet 2002;32:384–392. [PubMed: 12368912]

Hsu YM, Chou CY, Chen HH, Lee WY, Chen YF, Lin PW, Alper SL, Ellory JC, Shen MR. IGF-1 upregulates electroneutral K-Cl cotransporter KCC3 and KCC4 which are differentially required for breast cancer cell proliferation and invasiveness. J Cell Physiol 2007;210:626–636. [PubMed: 17133354]

Hu X, Hicks CW, He W, Wong P, Macklin WB, Trapp BD, Yan R. Bace1 modulates myelination in the central and peripheral nervous system. Nat Neurosci 2006;9:1520–1525. [PubMed: 17099708]

Jennings ML, Adame MF. Direct estimate of 1:1 stoichiometry of K(+)-Cl(-) cotransport in rabbit erythrocytes. Am J Physiol Cell Physiol 2001;281:C825–832. [PubMed: 11502559]

Karadsheh MF, Byun N, Mount DB, Delpire E. Localization of the KCC4 potassium-chloride cotransporter in the nervous system. Neuroscience 2004;123:381–391. [PubMed: 14698746]

Lang F, Busch GL, Ritter M, Volkl H, Waldegger S, Gulbins E, Haussinger D. Functional significance of cell volume regulatory mechanisms. Physiol Rev 1998;78:247–306. [PubMed: 9457175]

Lauf PK, Adragna NC. K-Cl cotransport: properties and molecular mechanism. Cell Physiol Biochem 2000;10:341–354. [PubMed: 11125215]

Menichella DM, Goodenough DA, Sirkowski E, Scherer SS, Paul DL. Connexins are critical for normal myelination in the CNS. J Neurosci 2003;23:5963–5973. [PubMed: 12843301]

Menichella DM, Majdan M, Awatramani R, Goodenough DA, Sirkowski E, Scherer SS, Paul DL. Genetic and physiological evidence that oligodendrocyte gap junctions contribute to spatial buffering of potassium released during neuronal activity. J Neurosci 2006;26:10984–10991. [PubMed: 17065440]

Mercado A, Vazquez N, Song L, Cortes R, Enck AH, Welch R, Delpire E, Gamba G, Mount DB. NH2-terminal heterogeneity in the KCC3 K+-Cl- cotransporter. Am J Physiol Renal Physiol 2005;289:F1246–F1261. [PubMed: 16048901]

Michailov GV, Sereda MW, Brinkmann BG, Fischer TM, Haug B, Birchmeier C, Role L, Lai C, Schwab MH, Nave KA. Axonal neuregulin-1 regulates myelin sheath thickness. Science 2004;304:700–703. [PubMed: 15044753]

Mount DB, Mercado A, Song L, Xu J, George AL Jr, Delpire E, Gamba G. Cloning and characterization of KCC3 and KCC4, new members of the cation-chloride cotransporter gene family. J Biol Chem 1999;274:16355–16362. [PubMed: 10347194]

Pearson MM, Lu J, Mount DB, Delpire E. Localization of the K(+)-Cl(-) cotransporter, KCC3, in the central and peripheral nervous systems: expression in the choroid plexus, large neurons and white matter tracts. Neuroscience 2001;103:481–491. [PubMed: 11246162]

Race JE, Makhlouf FN, Logue PJ, Wilson FH, Dunham PB, Holtzman EJ. Molecular cloning and functional characterization of KCC3, a new K-Cl cotransporter. Am J Physiol 1999;277:C1210–1219. [PubMed: 10600773]

Runker AE, Kobsar I, Fink T, Loers G, Tilling T, Putthoff P, Wessig C, Martini R, Schachner M. Pathology of a mouse mutation in peripheral myelin protein P0 is characteristic of a severe and early onset form of human Charcot-Marie-Tooth type 1B disorder. J Cell Biol 2004;165:565–573. [PubMed: 15148307]

Scherer SS, Xu YT, Nelles E, Fischbeck K, Willecke K, Bone LJ. Connexin32-null mice develop demyelinating peripheral neuropathy. Glia 1998;24:8–20. [PubMed: 9700485]

Shen MR, Chou CY, Ellory JC. Volume-sensitive KCI cotransport associated with human cervical carcinogenesis. Pflugers Arch 2000;440:751–760. [PubMed: 11007318]

Shen MR, Chou CY, Hsu KF, Liu HS, Dunham PB, Holtzman EJ, Ellory JC. The KCl cotransporter isoform KCC3 can play an important role in cell growth regulation. Proc Natl Acad Sci U S A 2001;98:14714–14719. [PubMed: 11724933]

Smith KJ, Blakemore WF, Murray JA, Patterson RC. Internodal myelin volume and axon surface area. A relationship determining myelin thickness? J Neurol Sci 1982;55:231–246. [PubMed: 7131033]

Trapp BD, Quarles RH, Suzuki K. Immunocytochemical studies of quaking mice support a role for the myelin-associated glycoprotein in forming and maintaining the periaxonal space and periaxonal cytoplasmic collar of myelinating Schwann cells. J Cell Biol 1984;99:594–606. [PubMed: 6204994]

Warner LE, Hilz MJ, Appel SH, Killian JM, Kolodry EH, Karpati G, Carpenter S, Watters GV, Wheeler C, Witt D, Bodell A, Nelis E, Van Broeckhoven C, Lupski JR. Clinical phenotypes of different MPZ (P0) mutations may include Charcot-Marie-Tooth type 1B, Dejerine-Sottas, and congenital hypomyelination. Neuron 1996;17:451–460. [PubMed: 8816708]

Yang Y, Allen E, Ding J, Wang W. Giant axonal neuropathy. Cell Mol Life Sci 2007;64:601–609. [PubMed: 17256086]

Yeiser EC, Rutkoski NJ, Naito A, Inoue J, Carter BD. Neurotrophin signaling through the p75 receptor is deficient in traf6-/- mice. J Neurosci 2004;24:10521–10529. [PubMed: 15548667]

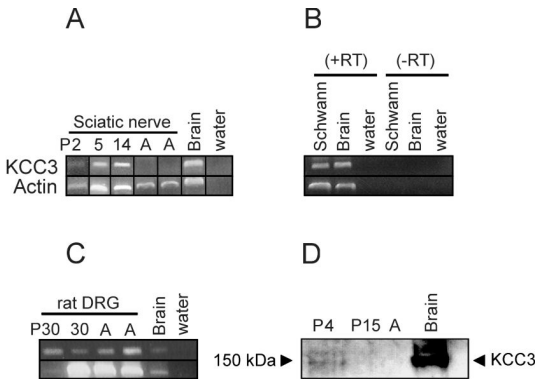

Figure 1. KCC3 is detected in sciatic nerves by semiquantitative RT-PCR and Western blot analysis

(A) Sciatic nerves from mouse pups (P2, P5, P14) but not adult are positive for KCC3 transcript. Mouse brain mRNA is used as positive control for KCC3, and actin primers are used as positive control for the PCR. Reactions with water (no cDNA) are negative. (B-C) KCC3 transcript is identified in rat cultured Schwann cells and rat DRG. Reactions without reverse trancriptase enzyme (-RT) are negative, indicating no DNA contamination. (D) Immunoblotting shows KCC3 protein expression in microsomes isolated from sciatic nerves at age P4, which are barely perceptible at P15, and undetectable in adult. Each lane was loaded with 35 μg microsomal protein, except for mouse brain positive control with 70 μg microsomal protein.

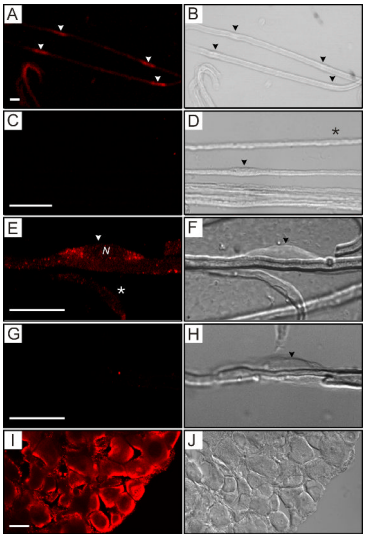

Figure 2. Positive immunolabeling of Schwann cells and DRG neurons with an anti-KCC3 antibody

(A) KCC3 immunostaining (red) of teased sciatic nerve fibers from wild-type mice at P8 shows punctate staining of Schwann cell bodies (arrowheads). (B) In the corresponding DIC image, arrowheads point to Schwann cell bodies, which appear as rounded protrusions along the fiber exterior. (C) Control panel, immunostaining with Cy3 secondary antibody alone, gives no signal. (D) Corresponding DIC image with arrowhead pointing to a Schwann cell body. (E) At higher magnification, the immunofluorescence shows a predominantly perinuclear distribution in the Schwann cell body. N = nucleus. This image reflects one plane of the Z-stack. The asterisk denotes a Schwann cell body lying in a different plane. (F) Corresponding DIC image. (G) Control panel, immunostaining of $KCC3^{-/-}$ fibers show absence of signal. (H) Corresponding DIC image. (I) Cryosectioned DRG (12 μm) shows strong KCC3 signal in sensory neurons. (J) The corresponding DIC image displays distinctive morphology of individual neurons. Scale bars = 20 μm.

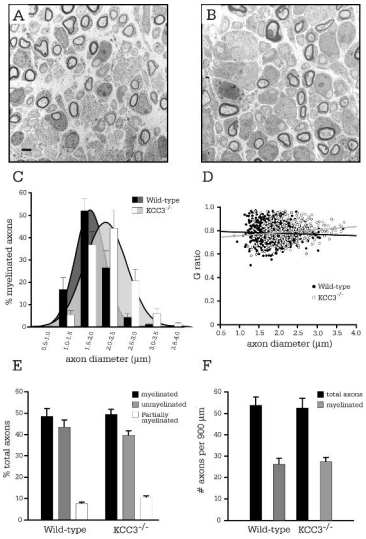

Figure 3. Myelination is normal in P3 KCC3$^{-/-}$ sciatic nerves, but axons are enlarged

(A) Electron micrograph of P3 KCC3$^{+/+}$ sciatic nerve. (B) KCC3$^{-/-}$ fibers are undistinguishable from their wild-type counterparts. Scale bar = 2μm. (C) Histogram analysis of axon diameter distributions reveals a shift to larger calibers for KCC3$^{-/-}$ axons. (D) G ratios are plotted as a function of axon diameter for both wild-type and KCC3$^{-/-}$ fibers. Note the increased size of the KCC3$^{-/-}$ axon population. (E) The percentage of myelinated, partially myelinated, and segregated unmyelinated (excluding Remak bundles) axons do not differ between wild-type and KCC3$^{-/-}$ mice. (F) The number of myelinated axons and total axons per unit area (axonal densities) are also equivalent between the two genotypes. (N = 4 per genotype)

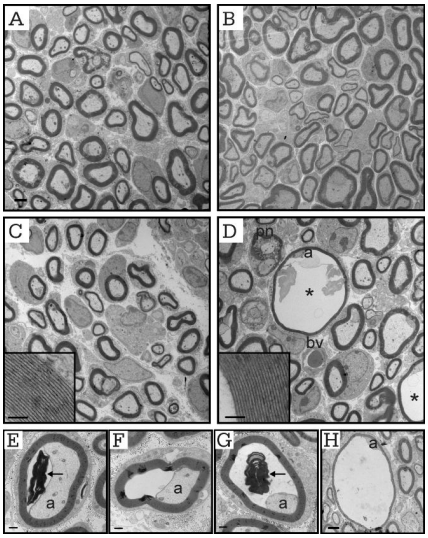

Figure 4. P8 KCC3$^{-/-}$ fibers exhibit abnormal periaxonal fluid accumulation

Electron micrographs of proximal sciatic nerve from wild-type (A) and mutant (B) mice. Electron micrographs of distal sciatic nerves of wild-type (C) and KCC3$^{-/-}$ (D) mice. Scale bar = 2 μm. Myelin compaction in mutant fibers (D, inset) is undistinguishable from that of wild-type (C, inset, scale bar = 500 nm). (D) Fibers with periaxonal fluid accumulation appear only in KCC3$^{-/-}$ nerves (asterisk). Note that even though the axon is still attached to the Schwann cell, it has lost most of its glial contacts. (E-H) Varying stages or degrees of severity of the abnormal fluid accumulation, which appear as an electron transparent region, in distal KCC3$^{-/-}$ sciatic nerve fibers. Scale bar = 500 nm. Note the presence of myelin debris (arrows) in the periaxonal space (E, G). These abnormal profiles were never seen in wild-type sciatic nerves. a = axon; pn = paranodes; bv = blood vessel.

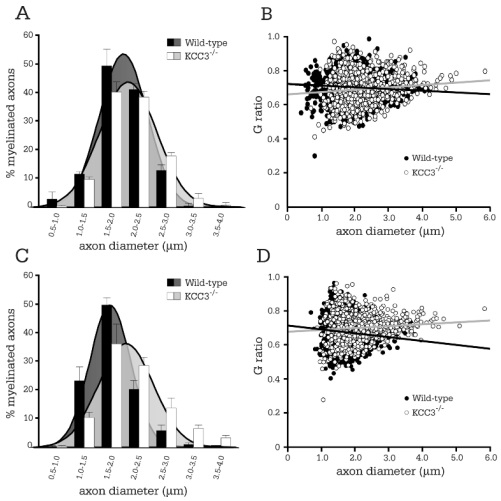

Figure 5. Increased axon diameters in P8 KCC3$^{-/-}$ fibers

(A) Histogram analysis of proximal sciatic nerve. Note the subtle but statistically significant (see Table 1) shift in axon diameter size. (B) G ratio scatter plot of proximal sciatic nerve. (C) Histogram analysis of distal sciatic nerve reveals an obvious shift in axon diameter for the mutant fibers. (D) Comparison of G ratio scatter plot regressions shows decreased myelin thickness in distal KCC3$^{-/-}$ sciatic nerve fibers. Fluid filled fibers were excluded from all graphs. (distal KCC3$^{+/+}$ N = 7; distal KCC3$^{-/-}$ N = 4; proximal KCC3$^{+/+}$ N = 4; proximal KCC3$^{-/-}$ N = 4)

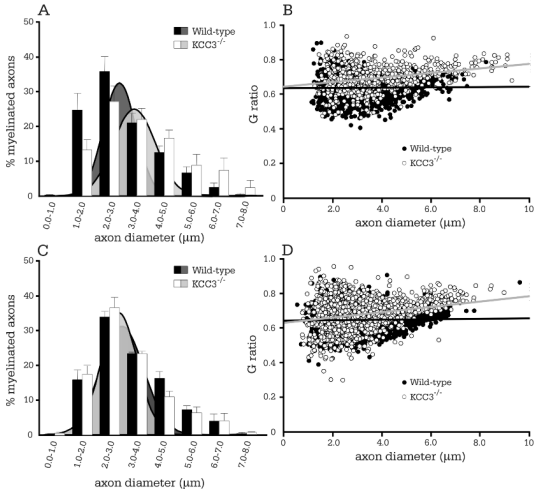

Figure 6. Proximal P30 KCC3$^{-/-}$ fibers are enlarged

(A) Histogram analysis of axon diameters reveal a population enlargement for proximal mutant fibers, indicating general swelling of axons. (B) Comparison of G ratio scatter plot regressions demonstrates the subtle reduction in myelin thickness in distal KCC3$^{-/-}$ sciatic nerve fibers. Fluid filled fibers were excluded from the plot. (C) Surprisingly, histogram plots of wild-type and mutant axon diameters overlapped, while (D) G ratio regression slope remained skewed for thinner myelin in mutant fibers. (distal KCC3$^{+/+}$ N = 3; distal KCC3$^{-/-}$ N = 3; proximal KCC3$^{+/+}$ N = 3; proximal KCC3$^{-/-}$ N = 3).

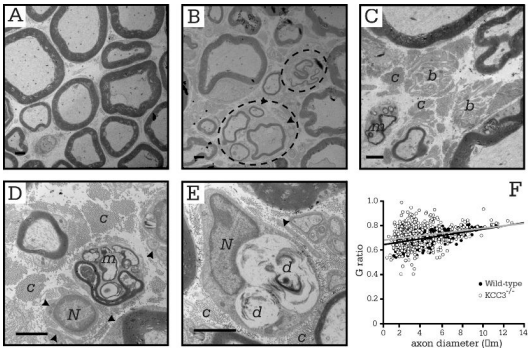

Figure 7. Myelin and axonal defects in adult KCC3$^{-/-}$ sciatic nerves

(A) Electron micrograph of wild-type sciatic nerve fibers with myelinated axons. (B-E) Electron micrographs of KCC3$^{-/-}$ nerve fibers showing macrophage invasion (m), bands of Büngner (b), signs of axon degeneration (d). Dashed ovals circling regenerating clusters. Note the abundance of collagen fibers (c) and redundant basal lamina (arrowheads). (F) G ratio plots are similar between KCC3$^{+/+}$ and mutant KCC3$^{-/-}$ fibers. N = nucleus, c = collagen, m = macrophage, d = degenerating axon. Scale bar = 2 μm. (KCC3$^{+/+}$ N = 2; KCC3$^{-/-}$ N = 2)

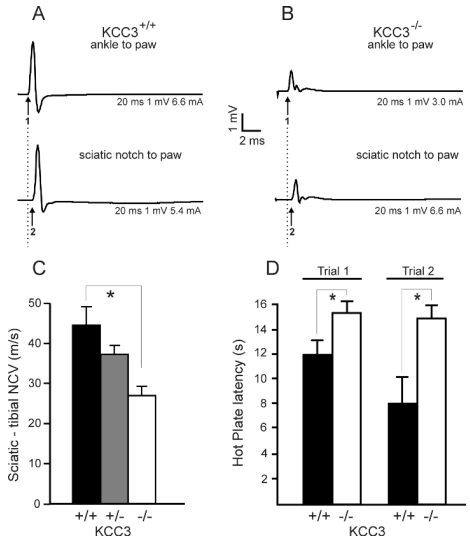

Figure 8. Neurophysiological assessment of KCC3$^{-/-}$ mice reveals decreased motorconduction velocities and decreased noxious pain sensitivity

Electromyograph traces from representative wild-type (A) and KCC3$^{-/-}$ (B) sciatic nerves. The top trace represents the compound muscle action potential (CMAP) measured at the foot muscles after stimulation at the ipsilateral knee, while the lower trace represents the CMAP measured at the same foot muscles (recording electrodes were not moved) after stimulation at the sciatic notch. Numbers 1 and 2 mark the onset of the CMAP. (C) Conduction velocity is significantly decreased in sciatic nerve from KCC3$^{-/-}$ mice. (KCC3$^{+/+}$ N = 5; KCC3$^{+/-}$ N = 6; KCC3$^{-/-}$ N = 4) Asterisks indicate statistical difference with $P < 0.001$. (D) KCC3$^{-/-}$ mice show increased latencies for pain response on the 52°C hot plate. Two trials were conducted, one week apart, yielding similar results. (KCC3$^{+/+}$ N = 12 ; KCC3$^{-/-}$ N = 6) Asterisks indicate statistical difference with $P < 0.001$.

Table I

Morphometric and conduction velocity data of KCC3 sciatic nerves

	N	Total myelinated fibers	Axon diameter (um)	G ratio	% periax. fluid
P3					
KCC3+/+	4	600	1.87 ± 0.09	0.774 ± 0.008	0
KCC3-/-	4	467	2.19 ± 0.09	0.783 ± 0.021	0.22
P value			0.0395 (s)	0.713 (ns)	
P8 Proximal					
KCC3+/+	7	1752	2.00 ± 0.34	0.699 ± 0.005	0
KCC3-/-	4	1131	2.24 ± 0.64	0.689 ± 0.007	1.23 ± 0.48
P value			< 0.05 (s)	> 0.05 (ns)	
P8 Distal					
KCC3+/+	4	1296	1.81 ± 0.07	0.665 ± 0.008	0
KCC3-/-	4	1128	2.18 ± 0.09	0.701 ± 0.007	2.55 ± 0.67
P value			< 0.05 (s)	< 0.05 (s)	
P30 Proximal					
KCC3+/+	3	1227	2.89 ± 0.10	0.645 ± 0.0020	0
KCC3-/-	3	710	3.93 ± 0.31	0.697 ± 0.0038	4.57 ± 2.3
P value			<0.05 (s)	<0.001 (s)	
P30 Distal					
KCC3+/+	3	2456	3.25 ± 0.13	0.651 ± 0.0012	0
KCC3-/-	3	1898	3.18 ± 0.23	0.675 ±0.0018	5.53 ± 3.8
P value			>0.05 (ns)	<0.001 (s)	
7-8 months					
KCC3+/+	2	498	3.86 ± 0.86	0.65 ± 0.0056	0
KCC3-/-	2	473	3.93 ± 0.10	0.67 ± 0.0097	1.14 ± 0.46
P value			0.61 (ns)	0.17 (ns)	
			NCV (m/s)		
KCC3+/+	5		44.7 ± 4.78		
KCC3-/+	6		37.5 ± 2.31		
KCC3-/-	4		28.6 ± 2.20		

(ns) not significant; (s) significant